A Shared-Aperture Dual-Band Dual-Polarized Filtering-Antenna-Array with Improved Frequency Response

Chun-Xu Mao, Steven Gao, *Member, IEEE*, Yi Wang, *Senior Member, IEEE*, Qi Luo, *Member, IEEE*, Qing-Xin Chu, *Senior Member, IEEE*

***Abstract*—In this paper, a novel dual-band dual-polarized (DBDP) array antenna with low frequency ratio and integrated filtering characteristics is proposed. By employing a dual-mode stub-loaded resonator (SLR) to feed and tune with two patches, the two feed networks for each polarization can be combined, resulting in the reduction of the feed networks and the input ports. In addition, owing to the native dual resonant features of the SLR, the proposed antenna exhibits 2nd-order filtering characteristics with improved bandwidth and out-of-band rejections. The antenna is synthesized and the design methodology is explained. The coupling coefficients between the SLR and the patches are investigated. To verify the design concept, a C/X-band element and a 2 × 2 array are optimized and prototyped. Measured results agree well with the simulations, showing good performance in terms of bandwidth, filtering, harmonic suppression and radiation at both bands. Such an integrated array design can be used to simplify the feed of a reflector antenna. To prove the concept, a paraboloid reflector fed by the proposed array is conceived and measured directivities of 24.6 dBi (24.7 dBi) and 28.6 dBi (29.2 dBi) for the X-polarization (Y-polarization) are obtained for the low- and high-band operations, respectively.**

***Index Terms*—Antenna array, dual-band, dual-polarized, filtering, integrated, stub-loaded resonator.**

I. Introduction

WIRELESS terrestrial and space/air-borne applications have an increase demand for the antenna with the features of dual-band dual polarizations [1]. Polarization diversity is usually desirable for enhancing the information content and combating the multi-path fading [2]-[3]. Dual-band or multi-band operations, on the other hand, could increase the versatility of the systems. For multifunction radar applications, different frequency operations are also required to share the same aperture in order to reduce the cost and weight of the RF frontend [4]-[6].

Manuscript submitted on June 29, 2016; This work is supported by the project "DIFFERENT" funded by EC FP7 (grant no. 6069923). YW is supported by UK EPSRC under Contract EP/M013529/1.

C. X. Mao, S. Gao and Q. Luo are with the School of Engineering and Digital Arts, University of Kent, UK. (e-mail: cm688@kent.ac.uk, s.gao@kent.ac.uk).

Y. Wang is with the Department of Engineering Science, University of Greenwich, UK.

Q. X. Chu is with the School of Electronic and Information Engineering, South China University of Technology, China.

Traditionally, dual-band operations of an antenna can be implemented by using two single-band elements or using one dual-band element. Employment of two single-band elements is always regarded more flexible for designing the dual-band antennas with high frequency ratios. In [4]-[8], perforated patches are used to design the dual-band arrays with dual polarizations characteristics while sharing the same aperture. In [9]-[13], the radiating elements with different resonant frequencies are interlaced for dual-band operations. One of the challenges in these array designs is the congestion of the feeding networks since each band and each polarization is usually excited separately. This would be much challenging as the frequency ratio decreases (much smaller than 2). To the best of the authors' knowledge, very few work has been reported focusing on the DBDP array with low frequency ratio.

To implement a DBDP array with a low frequency ratio, the dual-band element is believed to be more suitable. The main challenge of using a dual-band element is how to layout of the radiating elements to avoid grating lobes. Other challenges include complex feeding structures and mutual coupling between the two operation bands. A kind of combined feed is proposed to reduce the number of input ports [6]-[8]. However, these essentially involve separate feeding networks for each band then combined using a "duplexing" device with the assistance of the band-notch structures and matching stubs. The number of the feeding networks as well as the congestion are not reduced. Thus, they are not very suitable for solving the problems in low frequency ratio DBDP antenna design.

To overcome the problems, an integrated design concept is proposed in this paper. The integration of filter and antenna has been intensively investigated during the past several years [14]-[20]. In [20], an approach of using a multi-mode resonator to feed a patch for enhancing the bandwidth of the patch antenna is proposed. However, most of these works focus on single-band antenna. In this paper, the concept in [20] is further developed to design DBDP antenna with a low frequency ratio. By employing resonator as the feed of the antenna, not only the RF frontend can be simplified, but also the frequency responses of the antenna can be improved. In this work, two nested patches are coupled and tuned to a dual-mode stub-loaded resonator (SLR), generating two operation bands simultaneously. The coupling strengths between the SLR and the patches can be tuned by adjusting the position and the

dimension of the coupling slot. In addition, the antenna exhibits 2nd-order filtering characteristics at both bands with improved bandwidths and out-of-band rejections. A proof-of-concept 2 × 2 array is conceived, prototyped and measured. Such antenna can also be extended to a massive array or use as the feed of a reflector antenna.

This paper is organized as follows. Section II introduces the configuration of the DBDP element and its equivalent circuit. Section III details the design methodology. Section IV illustrates the proposed DBDP array. Section V presents the results and followed by the conclusion.

II. DBDP Antenna Element Design

A. Configuration

Fig. 1 shows the configuration of the proposed dual-band dual-polarized antenna element, which is composed of a stacked structure. The low and high band radiation elements are printed on the top- and bottom-layer of the upper substrate, respectively. As shown in Fig. 1(a), the low band antenna is a perforated patch with the perforation is large enough for allowing the radiation of the high band square patch. The size of the square patch is approximately a half-wavelength of the high band operation, whereas the perimeter of the perforated patch is about one wavelength of the low band operation. The two patches are nested in order to be fed by a common feed. For each polarization, a folded SLR is used to feed the two patches through a single slot in the ground. To improve the isolations and reduce the cross polarization, the two coupling slots for the each polarization are placed perpendicularly with each other.

Fig. 1(b) shows the configuration of the feeding networks printed on the bottom layer of the lower substrate. Because of its flexibility in controlling the resonant frequencies, the dual-mode SLR is used here so that it can be tuned with the two patches. The two resonant modes of the SLR can be derived using the odd- and even-mode method [20]-[22],

$$f_{odd} = \frac{c}{2*(2L_{r1}+L_{r3})\sqrt{\varepsilon_r}} \quad (1)$$

$$f_{even} = \frac{c}{2*(L_{r1}+L_{r2}+L_{r3}/2)\sqrt{\varepsilon_r}} \quad (2)$$

where c is the light velocity in the free space, ε_r is the effective dielectric constant, f_{odd} and f_{even} are the odd- and even-mode resonant frequencies of the SLR, respectively. In this design, f_{odd} is tuned with low-band perforated patch while f_{even} is tuned with the high-band square patch. Using the equation (1)-(2), the two resonant frequencies can be controlled independently by tuning the lengths of the resonator L_{r1}, L_{r2} and L_{r3}. Since the two bands of each polarization are fed using a single SLR in this design, the number of the feeding structures as well as the input ports can be reduced by a half.

The stacked configuration of the antenna is shown in Fig. 1(c). A Rohacell 51HF foam with a thickness of 2 mm is inserted between the two substrates as a spacer to improve the antenna impedance matching and bandwidths. RT/Duriod 4003C substrate with a relatively dielectric constant of 3.55 and

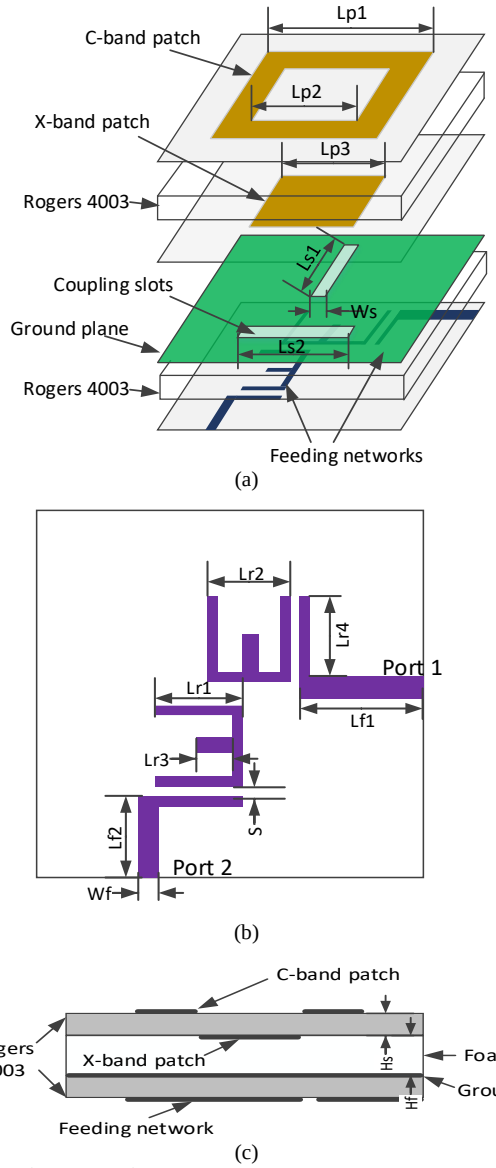

Fig. 1. Configuration of the proposed DBDP element: (a) exploded view, (b) bottom view, (c) side view.

TABLE I
PARAMETERS OF THE PROPOSEDANTENNA: (MM)

Lp1	Lp2	Lp3	Lp4	Ls1	Ls2	Ws	Lf1	Lf2
14.5	9	7.8	3	7.2	10	0.5	11.8	8.4
Wf	Lr1	Lr2	Lr3	Lr4	S	Hs	Hf	
1.8	5.5	6	2	5.5	0.3	0.813	2	

loss tangent of 0.0027 is used in the design. High Frequency Simulation Software (HFSS 15) is employed to perform the simulations and the optimized parameters are listed in Table I.

B. Topology and synthesis

The proposed dual-band element for each polarization can be represented and synthesized using a coupled resonator-based topology, as shown in Fig. 2. The two patches can be regarded as two single-mode resonators or a dual-mode resonator with corresponding resonant frequencies of f_1 and f_2, respectively. The odd- and even-mode of the SLR are also tuned to resonate at

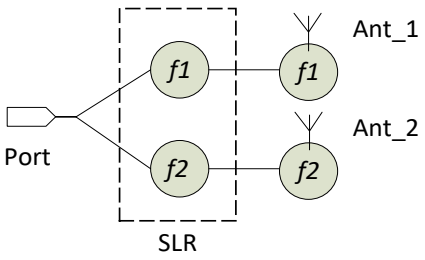

Fig. 2. The equivalent resonator-based topology of the proposed dual-band filtering antenna at each polarization.

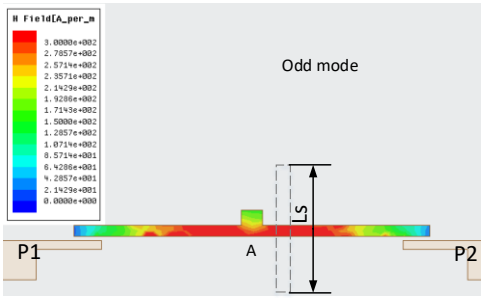

(a)

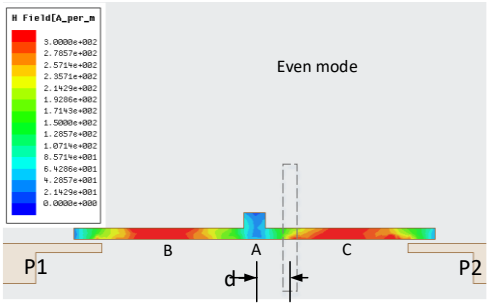

(b)

Fig. 3. Tangential magnetic-field distribution on the surface of an unfolded SLR: (a) the odd-mode resonance at 5.2 GHz and (b) the even-mode resonance at 10 GHz.

f_1 and f_2. Then the SLR and the two patches are electromagnetically coupled, forming two separate passbands with 2nd-order filtering responses. The two passbands of each polarization are excited simultaneously. The lines between the resonators in the topology represent the coupling between the resonators. As an example to implement a DBDP antenna with low frequency ratio (less than 2), the frequency specifications of the dual-band antenna are given as follows,

Low band: f_1 = 5.2 GHz, BW = 200 MHz

High band: f_2 = 10 GHz, BW = 500 MHz

The coupling coefficients and the external quality factors can be derived,

Low band: $m_{1,2}$ = 0.031, Q_{ext} = 45.1

High band: $m_{1,2}$ = 0.051, Q_{ext} = 27.2

where $m_{i,j}$ is the coupling coefficient between the resonator i and j.

III. Methodology

A. Coupling

In this integrated design, the two patches can be fed by the SLR through electromagnetic coupling only if the two patches are tuned with the dual modes of the SLR, respectively. Fig. 3 shows the simulated tangential magnetic-field distribution of an unfolded SLR corresponding to the odd- and even-mode resonance. As can be observed in Fig. 3(a), the SLR has the strongest magnetic-field distribution at its central part (denoted as point A) when the odd-mode is excited (low-band operation). It is noted that the dashed rectangle indicates the location of the coupling slot where the power is transferred to the patches through a coupling. When the even-mode is excited (high-band operation), there are two magnetic-field maxima, as the point B and C indicated in Fig. 3(b). On the contrary, point A becomes the minima. By positioning the slot between A and C, the electromagnetic energy can be coupled to the two patches simultaneously.

The coupling strengths at the two operation bands can be tuned by adjusting the relative coupling positions (d) and the dimension of the coupling slot [19]. According to experimental studies, the approximate equations for evaluating coupling strengths can be derived,

$$M_{f1} \approx \frac{A_1 \cdot Ls \cdot Ws}{d} \tag{3}$$

$$M_{f2} \approx A_2 \cdot Ls \cdot Ws \cdot d, \qquad \text{A} < \text{d} < \text{C}, \tag{4}$$

where, M_{f1} and M_{f2} are the mutual couplings between the SLR and the patch at f_1 and f_2; Ls is the length of the coupling slot; Ws is the width of the coupling slot; d is coupling position, which is situated between the point A and C. A_1 and A_2 are the corresponding constants. As can be observed, the mutual couplings are proportional to the length and width of the coupling slot. At the low-band (f_1), M_{f1} is inversely proportional to the d. At the high-band (f_2), M_{f2} is proportional to the d.

By using full-wave simulations, the corresponding coupling coefficients between the SLR and the patches can be evaluated using the following expression [20]-[21],

$$M_{ij} = \frac{f_j^2 - f_i^2}{f_j^2 + f_i^2} \tag{5}$$

where f_i and f_j are the two resonant frequencies of the 2nd-order coupled SLR-patch for each band operation. Fig. 4 presents the coupling coefficients between the SLR and the two patches corresponding to different lengths of the slot (denoted as Ls) and the locations of the slot (denoted as d in Fig. 3). As can be seen, the dimension of the slot has a similar influence on the coupling strength at both bands. But the variation of the coupling coefficients between the SLR and the square patch (high band operation) is more significant than that of the low-band. In contrast, changing the locations of the coupling slot has a reverse effect on the two bands, as shown in Fig. 4(b). This disparate relationship provides another degree of freedom to obtain the coupling coefficients required for the two bands.

B. 2nd-order filtering characteristics

Owing to the dual-mode SLR is coupled and tuned with two single-mode patches, 2nd-order filtering characteristics at the both bands can be achieved. The advantages of this coupling structure can be appreciated by the comparison with the case that fed by a microstrip line. Fig. 5 shows the simulated S-parameters of the coupled SLR-fed antenna and a counterpart

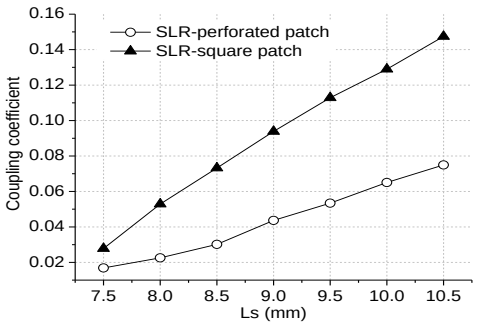

(a)

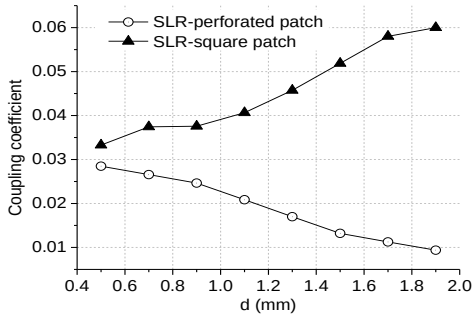

(b)

Fig. 4. Coupling coefficients between the SLR and the two patches with different (a) length of slot *Ls*, (b) location of the slot *d*.

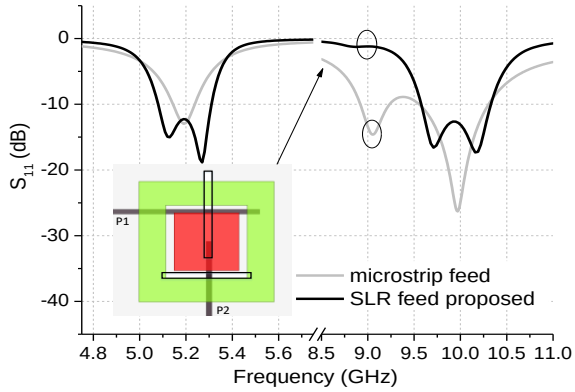

Fig. 5. S-parameters comparison between the SLR-feed dual-band antenna and a microstrip feed dual-band antenna.

fed by microstrip. It should also be noted that the results of the microstrip-fed antenna at the two bands are obtained separately as different lengths of the microstrip are required to achieve impedance matching at two bands. It is observed that the proposed SLR-fed antenna exhibits a 2nd-order filtering characteristics with improved bandwidth and out-of-band rejection as compared with the counterpart of microstrip-fed. For the microstrip-fed antenna, only one resonant frequency can be seen in the low band and the fractional bandwidth (FBW) is only 1.9%. However, when the patches are fed using the resonator, two resonant frequencies are generated at both bands, resulting in wider bandwidth (FBW = 4.6 %).

The current distribution at the two operation bands is shown in Fig. 6. As can be observed, strong current flows along the perforated patch at the low band operation. The current on the inner square patch is very weak. However, when the antenna works at high band, the square patch is excited with intensive current distribution. In contrast, the current on the perforated

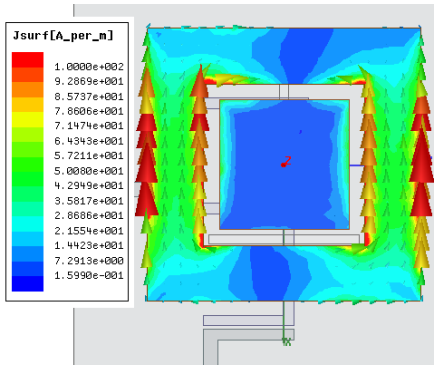

(a)

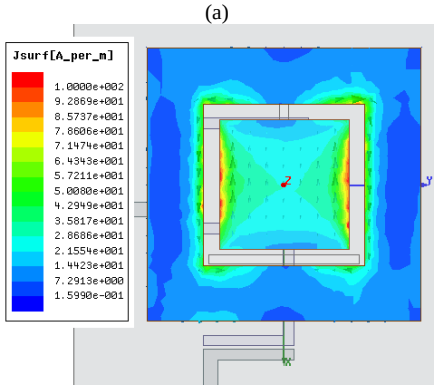

(b)

Fig. 6. Current distribution at two bands: (a) 5.2 GHz, (b) 10 GHz.

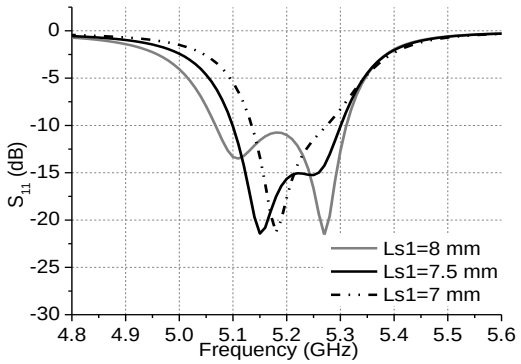

(a)

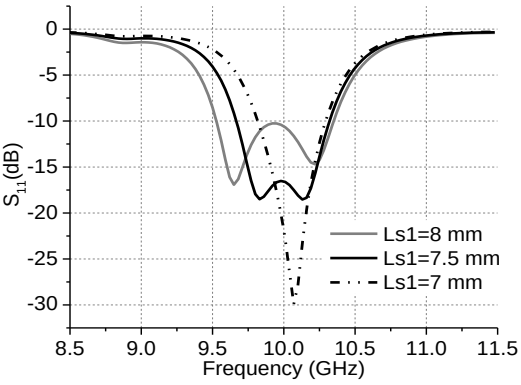

(b)

Fig. 7. The variation of bandwidths with different lengths of the slot *Ls1*: (a) low band, (b) high band.

patch is very weak except from the circle area of the perforation. The current distribution demonstrates that the perforated patch operates at low band whereas the inner square

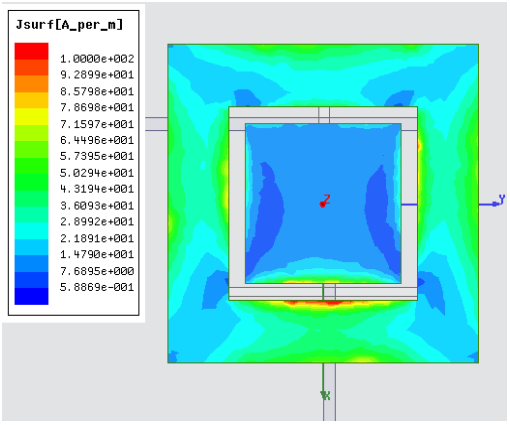

(a)

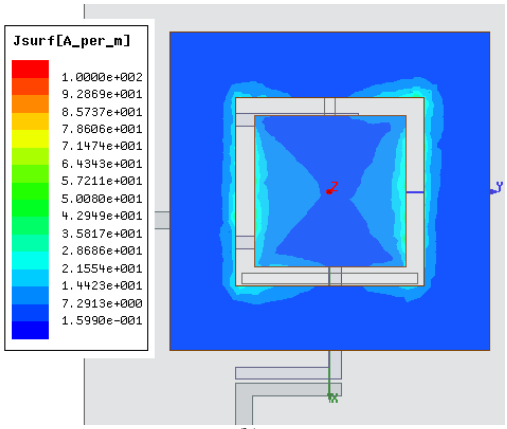

(b)

Fig. 8. The current distributions at 9 GHz of the two dual-band antennas with different feeds: (a) microstrip feed, (b) SLR feed.

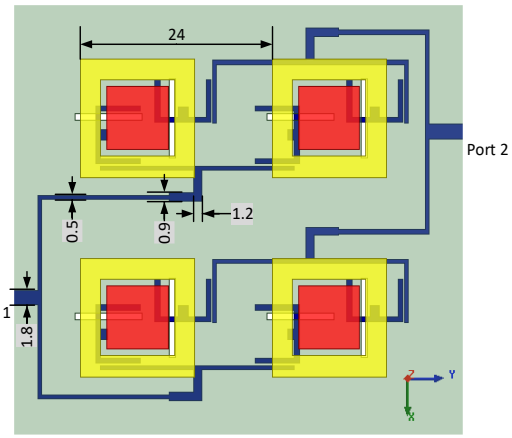

Fig. 9. The layout of the proposed 2 × 2 DBDP filtering antenna array: (unit: mm).

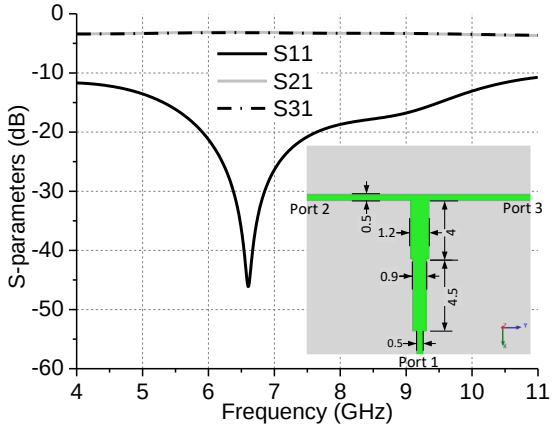

Fig. 10. The simulated S-parameters of the stepped two-way power divider: (unit: mm).

patch works at the high band. The mutual coupling between the two patches is considerable weak.

Another feature of the SLR-fed antenna is that the bandwidths at the both operations can be controlled by adjusting the coupling coefficient between the SLR and the two patches. Using the results presented in Fig. 4, the coupling coefficients can be adjusted by changing the dimensions of the coupling slot. Thus, the bandwidths can be controlled correspondingly. Fig. 7 shows the variation of the bandwidths at both bands with different lengths of the coupling slot. As can be observed, when the *Ls1* is less than 7 mm, the two reflection zeros in each band are merged together. When the length increases from 7 to 8 mm, the two reflection zeros emerge and the bandwidths are increased from 150 to 250 MHz (500 to 800 MHz) for the low band (high band) operations.

C. Harmonic suppression

The proposed antenna has another advantage of harmonic suppression, as also shown in Fig. 5. For the microstrip-fed antenna, a 2nd-order harmonic is emerged at around 9 GHz, causing the channel interference for the high band operation. However, when the patches are fed by the resonator, the harmonic can be significantly suppressed with the return loss suppressed from 15 to 2 dB. This harmonic suppression is attributed to the integration of the filtering and the radiating devices that only the frequencies that match the two resonant frequencies of the SLR can be transmitted/received. To verify the harmonic suppression performance, simulated current distribution at 9 GHz is presented, as shown in Fig. 8. It can be observed from Fig. 8(a), 2nd-order harmonic is stimulated on the perforated patch with strong current flowing on the patch when the antennas are fed by microstrip. However, when the antennas are fed by SLR, the current on the perforated patch is significantly reduced and the 2nd-order harmonic is suppressed, as presented in Fig. 7(b). Such filtering characteristics is useful for reducing the interferences from unwanted channels.

IV. DBDP Filtering Array

The presented DBDP filtering antenna element can be extended to conceive antenna array. To verify this concept, a 2 × 2 array is designed, as shown in Fig. 9. The two bands for each polarization are combined using an SLR and fed by a power dividing network, resulting in the reduction of the number of the coupling slots, feed networks and input ports. Thus, only two feed networks are employed to feed the DBDP array. This reduction is very useful for simplifying the complexity of the designs of the dual-band antenna arrays with dual polarizations. This improvement is very useful to design a shared-aperture DBDP array with a low frequency ratio.

One of the problems to be solved in this integrated DBDP array is that a wideband dividing network is required to evenly feed the radiation elements. To overcome this problem, a 2-way T-junction power divider with stepped quarter wavelength transformer is conceived. Fig. 10 shows the configuration of the

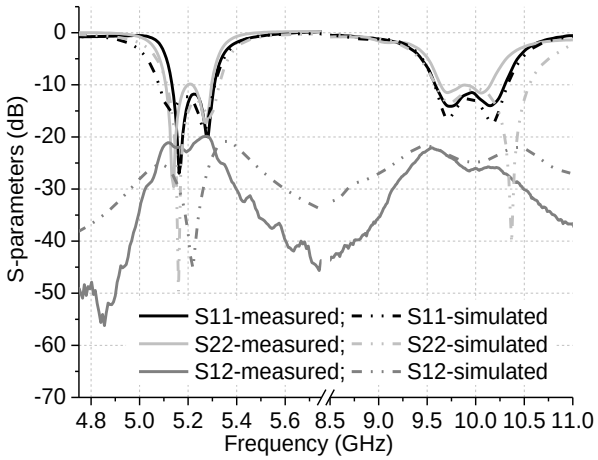

Fig. 11. Measured and simulated S-parameters of the DBDP element.

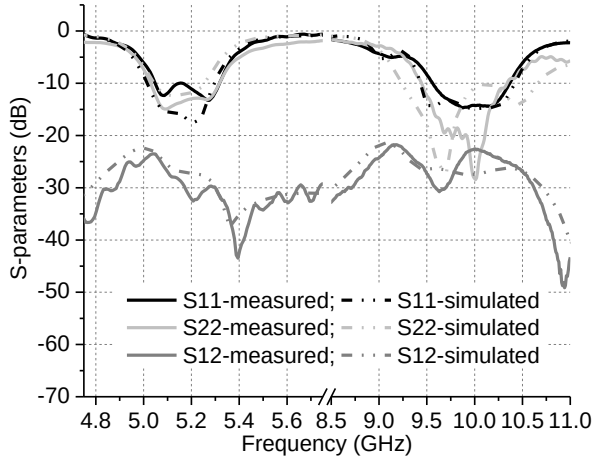

Fig. 12. Measured and simulated S-parameters of the DBDP filtering antenna array.

2-way power divider and the corresponding simulated S-parameters. The stepped quarter-wavelength impedance transformer is used for broadening the operation bandwidth. As can be observed, the power divider has a very wide bandwidth, covering the C- and X-band simultaneously. The insertion loss is about 3.4 dB at the both two operation bands, including the 3 dB power division loss.

Another issue to be concerned is that the spacing between the elements. Since the dual-band element is adopted in this work, the two antenna arrays have an identical physical spacing between the radiating elements, leading to grating lobes at the high band operation. Here, the dual bands are designed at C- and X-band (frequency ratio is about 2) as an example to verify the concept. Since the DBDP antenna with low frequency ratio (much lower than 2) is the target of this design, the problem of grating lobes could be alleviated as the frequency ratio decreases. In this design, the spacing between the radiating elements is selected as 24 mm, i.e. 0.42 and 0.8 wavelength at 5.2 and 10 GHz, respectively.

V. Results And Discussion

A. Element and array

The proposed DBDP filtering antenna element and the array were prototyped and measured. Fig. 11 shows the simulated

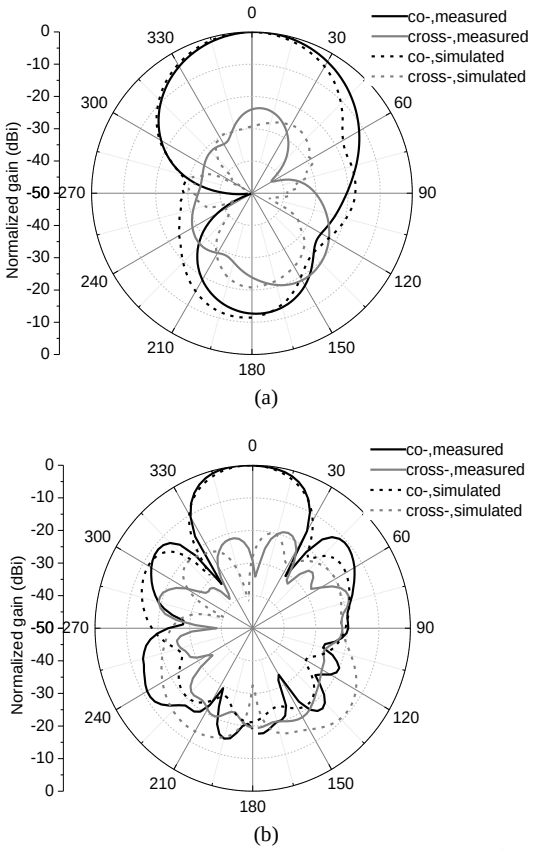

Fig. 13. Normalized simulated and measured radiation patterns of the 2 × 2 DBDP antenna when port 1 is excited: (a) 5.2 GHz, (b) 10 GHz.

and measured S-parameters of the proposed DBDP element. It can be seen that the measured results agree reasonably well with the simulations in a broadband. For each input port, two operation bands are obtained. At the low band operation, an impedance bandwidth from 5.1 to 5.3 GHz is achieved at two polarizations. At the high band, the antenna exhibits a bandwidth from 9.6 to 10.2 GHz. The antenna element exhibits 2nd-oder filtering characteristics with two reflection zeros are produced at both bands. These reflection zeros are beneficial to increase the bandwidths while shaping sharp roll-off at the both edges of the two bands. Out-of-the-band, the antenna shows an excellent harmonic suppression performance with the return loss close to 0 dB. The antenna also exhibits good isolation between the two polarizations with the measured $|S_{21}|$ is lower than -20 dB and -24 dB in the low and high bands, respectively. The discrepancy between the simulated and measured results is caused by the air-gap and misalignment between the substrates when assembling the antenna.

Fig. 12 shows the simulated and measured S-parameters of the 2 × 2 DBDP array. The measured results agree with the simulations. The array shows two operation bands from 5.05 to 5.3 GHz and from 9.6 to 10. 3 GHz, respectively. The measured isolations between the two polarizations are over 25 dB and 23 dB in the low and high bands. Compared with the results in Fig.11, the array shows wider bandwidths than the element at both bands, which may be contributed to the influence of the power dividing networks. The discrepancy between the simulations and measurements is mainly caused by the misalignment in the process of assembling multiple substrates.

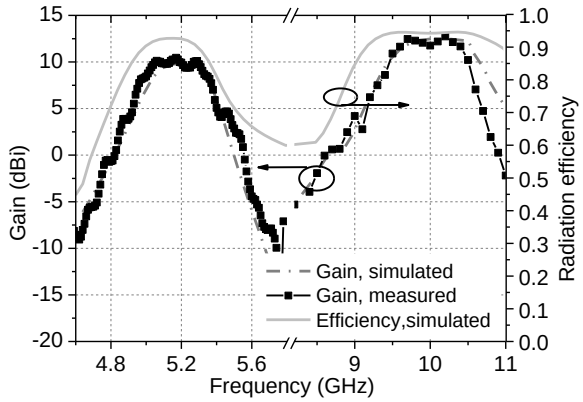

Fig. 14. Simulated and measured gains and the simulated radiation efficiency of the 2 × 2 C/X-band filtering array.

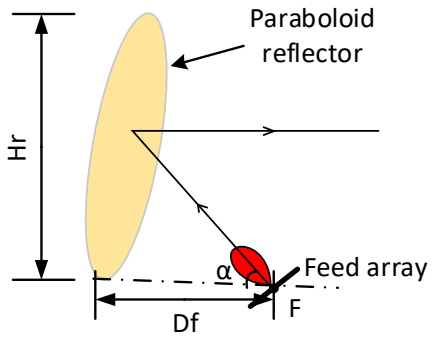

Fig. 15. The geometry of the offset paraboloid reflector antenna system. *Hr* = 300 mm, *Df* = 300 mm.

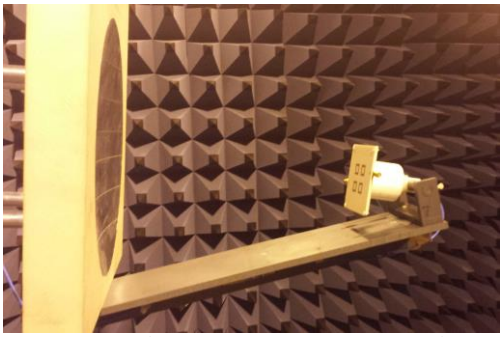

Fig. 16. The proposed feed array and the paraboloid reflector antenna under measurement.

The radiation patterns of the array in two orthogonal polarizations were measured with one of the ports was excited and the other was terminated with a 50 Ω load. Fig. 13 shows the normalized simulated and measured radiation patterns of the 2 × 2 DBDP array. As can be seen, the measured results agree well with the simulated ones, showing the main beam in the broadside direction. The measured cross polarizations are lower than -24 and -26 dB at 5.2 GHz and 10 GHz, respectively. The minor difference between the simulated and measured results is attributed to influence of the cables and other materials used in the measurement.

Fig. 14 shows the simulated and measured gains and the simulated radiation efficiency of the 2 × 2 antenna array. It is observed that the measured and simulated gains agree very well with each other. The antenna exhibits a flat gain responses of 10 dBi and 12 dBi at the low and high bands, respectively. Out of

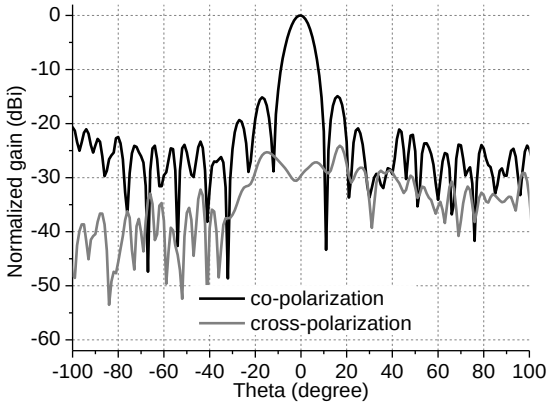

(a)

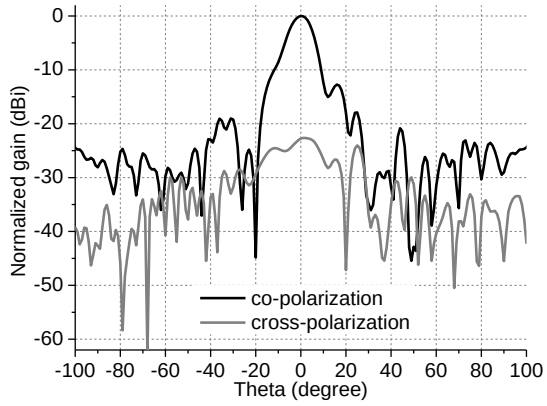

(b)

Fig. 17. The measured normalized co- and cross- polarization radiation patterns of the paraboloid reflector antenna at 5.2 GHz: (a) X-polarization, Port-1 excitation, (b) Y-polarization, Port-2 excitation.

the two bands, the gains rapidly decrease to below 0 dBi as the frequency is below 4.7 GHz (8.8 GHz) and above 5.6 GHz (10.9 GHz) for the low band (high band) operation. The rapid decrease of the gain demonstrates that the antenna has good filtering characteristics. The minor discrepancy between the simulated and measured results occurs at the high-band over 10.5 GHz, which is mainly attributed to the errors of the measurement equipment. At the two operation bands, the simulated radiation efficiencies are above 90%.

B. Array-fed paraboloid reflector antenna

The proposed integrated filtering antenna can not only use as a standalone device, but also serves as a planar feed of a reflector antenna. Fig. 15 shows the geometry of a paraboloid reflector. The paraboloid reflector is illuminated using the proposed 2 × 2 DBDP array, which is placed at the focal point with its aperture faces the center section of the reflector. The reflector has a diameter (*Hr*) of 300 mm and the focal length (*Df*) of 300 mm which is about 5 and 10 wavelengths at the 5.2 and 10 GHz, respectively. The reflector antenna system under measurement is shown in Fig. 16.

Fig. 17 shows the normalized measured co- and cross-polarization patterns of the reflector antenna at 5.2 GHz. The antenna shows a good radiation performance with the main beam in the broadside. When port 1 is excited (X-polarization), the antenna has a half-power beam width (HPBW) of 10.4 degrees and the directivity of the antenna can be calculated as

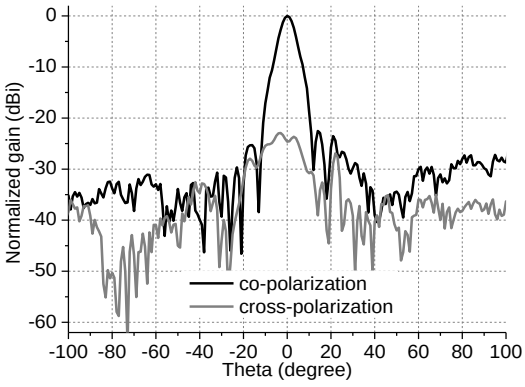

(a)

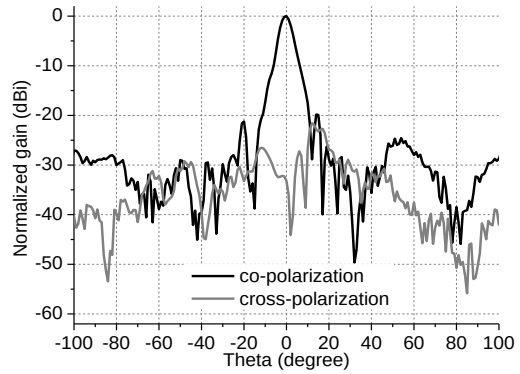

(b)

Fig. 18. The measured normalized co- and cross- polarization radiation patterns of the paraboloid reflector antenna at 10 GHz: (a) X-polarization, Port-1 excitation, (b) Y-polarization, Port-2 excitation.

24.7 dBi. The side lobe is below -15 dB and the cross polarization discrimination (XPD) is over 29 dB in broadside. For the Y-polarization, an HPBW of 10.6 degrees is achieved and the calculated directivity is 24.6 dBi. The side lobe is lower than -14 dB and the XPD is over 23 dB. Compared with the X-polarization, the radiation performance is slightly deteriorated, which is caused by the misaligning between the reflector and the feed when mounting the antenna.

Fig. 18 shows the normalized measured co- and cross-polarization patterns of the reflector antenna at 10 GHz. Due to the increase of the electrical size at high hand operation, the antenna exhibits a narrower HPBW and higher directivity. When port 1 is excited (X-polarization), the antenna has an HPBW of 6.7 degrees and the directivity is calculated as 28.6 dBi. The side-lobe is below -24 dB and the XPD is over 25 dB. For Y-polarization, the HPBW is about 6.2 degrees and the calculated directivity is 29.2 dBi. The side lobe is below -20 dB and the XPD is over 33 dB.

VI. Conclusion

In this paper, a novel design concept of integrating SLR in antenna design is presented for implementing the dual-band dual-polarized array with low frequency ratio and filtering characteristics. Thanks to the dual-mode SLR is used to couple and tune with a dual-band patch, the antenna exhibits 2nd-order filtering feature with improved bandwidth and out-of-band rejection. Another advantage of this work is that the coupling slots, feed networks and the input ports can be reduced by 50%, which is beneficial to alleviate the congestion of the feeding networks. Such design concept is very useful in DBDP array design with a frequency ratio much lower than 2. To verify the concept, a C/X-band element and a 2 × 2 array are conceived. Simulated and measured results agree well with each other, showing good performance in terms of bandwidths, isolations, radiation patterns and antenna gains at both bands. Such integrated design can not only be used in the massive array, but also use as the feed of a reflector antenna.

References

[1] W. Imbriale, S. Gao and L. Boccia (eds), Space Antenna Handbook, 2012: Wiley.

[2] C. X. Mao and Q. X. Chu, "Compact co-radiator UWB-MIMO antenna with dual polarization," *IEEE Trans. Antennas and Propag.*, vol. 62, no. 9, pp. 4474-4480, Sep. 2014.

[3] S. Gao, L. W. Li, M. S. Leong and T. S. Yeo, "Dual-polarized slot-coupled microstrip antenna with wide bandwidth," *IEEE Trans. on Antennas and Propagation*, vol. 51, no. 3, pp. 441-448, Mar. 2003.

[4] L. Shafai, W. Chamma, M. Barakat, P. Strickland and G. Seguin, "Dual-Band Dual-Polarized Perforated Microstrip Antennas for SAR Application," *IEEE Trans. Antennas and Propag.*, vol. 48, no. 1, pp. 58-66, Jan. 2000.

[5] D. M. Pozar, S. D. Targonski, "A Shared-Aperture Dual-Band Dual Polarized Microstrip Array," *IEEE Trans. Antennas and Propag.*, vol. 49, no. 2, pp. 150-157, Feb. 2001.

[6] T. W. Chiou and K. L. Wong, "A Compact Dual-Band Dual-Polarized Patch Antenna for 900/1800-MHz Cellular Systems," *IEEE Trans. Antennas Propag.*, vol. 51, no. 8, pp. 1936-1940, Jan. 2003.

[7] G. Vetharatnam, C. B. Kuan and C. H. Teik, "Combined Feed Network for a Shared-Aperture Dual-Band Dual-Polarized Array," *IEEE Micro. and Wireless Components Lett.*, vol. 4, pp. 297-299, 2005.

[8] S. Soodmand, "A novel circular shaped dual-band Dual-polarized Patch antenna and introducing a new approach for designing combined feed networks", Presented at 2009 Loughborough Antennas & Propagation Conference, LAPC 2009, pp. 401-404.

[9] R. Pokuls, J. Uher and D. M. Pozar, "Dual-Frequency and Dual-Polarization Microstrip Antennas for SAR Application," *IEEE Trans. Antennas and Propag.*, vol. 46, no. 9, pp. 1289-1296, Sep. 1998.

[10] Z. Yang and K. Warnick, "Multiband dual-polarization high-efficiency array feed for Ku/reverse-band Satellite communications," *IEEE Antennas Wireless Propag*., vol. 13, pp. 1325-1328, 2014.

[11] H. Moghadas, M. Daneshmand and P. Mousavi, "A dual-band high-gain resonant cavity antenna with orthogonal polarizations," *IEEE Antennas Wireless Propag*., vol. 10, pp. 1220-1223, 2011.

[12] K. Naishadham, R. Li, L. Yang, T. Wu, W. Hunsicker, M. Tentzeris, "A shared-aperture dual-band planar array with self-similar printed folded dipoles," *IEEE Trans. Antennas Propag.*, vol. 61, no. 2, pp. 606-613, Feb. 2013.

[13] S. S. Zhon, Z. Sun, L. B. Kong, C. Gao, W. Wang and M. P. Jin, "Tri-band dual-polarization shared-aperture microstrip array for SAR application," *IEEE Trans. Antennas Propag.*, vol. 60, no. 9, pp. 4157-4165, Sep. 2012.

[14] C. X. Mao, S. Gao, Z. P. Wang, Y. Wang, F. Qin, B. Sanz and Q. X. Chu, "Integrated Filtering-Antenna with Controllable Frequency Bandwidth," *9th European Conf. on Antenna and Propag*., pp. 1-4, 2015.

[15] Z. H. Jiang, D. Werner, "A compact, wideband circularly polarized co-designed filtering antenna and its application for wearable devices with low SAR," *IEEE Trans. Antennas and Propag.*, vol. 63, no. 9, pp. 3808-3818, Sep. 2015.

[16] X. Y. Zhang, W. Duan and Y. M. Pan, "High-gain filtering patch antenna without extra circuit," *IEEE Trans. Antennas and Propag.*, vol. 63, no. 12, pp. 5883-5888, Dec. 2015.

[17] J. Wu, Z. Zhao, Z. Nie and Q. Liu, "A printed unidirectional antenna with improved upper band-edge selectivity using a parasitic loop," *IEEE Trans. Antennas and Propag.*, vol. 63, no. 4, pp. 1832-1837, Apr. 2015.

[18] A. I. Abunjaileh, I. Hunter and A. Kemp, "A circuit-theoretic approach to the design of quadruple-mode broadband microstrip patch antenna," *IEEE Trans. Microw. Theory Tech*., vol. 56, no. 4, pp. 896-890, Apr. 2008.

[19] C. K. Lin and S. J. Chung, "A Filtering Microstrip Antenna Array," *IEEE Trans. Microw. Theory Tech., vol.* 59, no. 11, pp. 2856-2863, Mar. 2011.
[20] C. X. Mao, S. Gao, Y. Wang, F. Qin and Q. X. Chu, "Multi-Mode Resonator-Fed Dual Polarized Antenna Array with Enhanced Bandwidth and Selectivity," *IEEE Trans. Antennas and Propag.*, vol. 63, no. 12, pp. 5492-5499, Dec. 2015.
[21] X. Y. Zhang, J. X. Chen, Q. Xue and S. M. Li, "Dual-band Bandpass Filters Using Stub-Loaded Resonators," *IEEE Micro. and Wireless Components Lett.*, vol. 17, No. 8, pp. 583-585, Aug. 2007.
[22] J. S. Hong and M. J. Lancaster, *Microwave Filter for RF/Microwave Application*. New York: Wiley, 2001.